Mon. Not. R. Astron. Soc. **000**, 1–9 (2009) Printed 20 December 2010 (MN LATEX style file v2.2)

Characterisation of red-giant stars in the public *Kepler* data

S. Hekker[1⋆], R.L. Gilliland[2], Y. Elsworth[1], W.J. Chaplin[1], J. De Ridder[3], D. Stello[4], A. Miglio[5], T. Kallinger[6,7], K.A. Ibrahim[8], T.C. Klaus[8], J. Li[9]

[1]*School of Physics and Astronomy, University of Birmingham, Edgbaston, Birmingham B15 2TT, UK*
[2]*Space Telescope Science Institute, 3700 San Martin Drive, Baltimore, MD 21218, USA*
[3]*Instituut voor Sterrenkunde, K.U. Leuven, Celestijnenlaan 200D, 3001 Leuven, Belgium*
[4]*Sydney Institute for Astronomy (SIfA), School of Physics, University of Sydney, NSW 2006, Australia*
[5]*Institut d'Astrophysique et de Géophysique, Université de Liège, Allée du 6 Août, 4000 Liège, Belgium*
[6]*Department of Physics and Astronomy, University of British Colombia, 6224 Agricultural Road, Vancouver, BC V6T 1Z1, Canada*
[7]*Institute for Astronomy, University of Vienna, Türkenschanzstrasse 17, A-1180 Vienna, Austria*
[8]*Orbital Sciences Corporation/NASA Ames Research Center, Moffett Field, CA 94035, USA*
[9]*SETI Institute/NASA Ames Research Center, Moffett Field, CA 94035, USA*

Received; accepted

ABSTRACT

The first public release has now been made of long-cadence stellar photometric data collected by the NASA *Kepler* mission. In this paper we aim to characterise the red-giant (G-K) stars in this large sample in terms of their solar-like oscillations. We use published methods and well-known scaling relations in the analysis. Just over 70% of the red giants in the sample show detectable solar-like oscillations, and from these oscillations we are able to estimate the fundamental properties of the stars. This asteroseismic analysis reveals different populations: low-luminosity H-shell burning red-giant branch stars, cool high-luminosity red giants on the red-giant branch and He-core burning clump and secondary-clump giants. Furthermore, the detection of solar-like oscillations in red giants does not depend on the long-term variability of the stars.

Key words: asteroseismology – methods: observational – techniques: photometric – stars: late type

1 INTRODUCTION

The NASA *Kepler* satellite (Borucki et al. 2009) was launched successfully in March 2009 into an earth-trailing orbit. The satellite is observing ∼150 000 stars simultaneously with high-precision photometry at a near-regular cadence of 29.4 minutes. Data taken during the first 10 day run (Q0), which lasted from 2 May 2009 until 11 May 2009 and the consecutive 33 day run (Q1 13 May 2009 - 15 June 2009) have been made public[1]. These data have been processed using the *Kepler* science processing pipeline Jenkins et al. (2010a) and have been characterised in terms of their stellar parameters and variability by Ciardi et al. (2010). In this work we characterise the red-giant stars using asteroseismology, i.e., the data have been analysed to search for solar-like oscillations. For a recent review of solar-like oscillations in red-giant stars we refer to Hekker (2010), while the following papers present recent results from the *Kepler* (e.g., Bedding et al. 2010; Huber et al. 2010; Kallinger et al. 2010a; Hekker et al. 2010d) and CoRoT (e.g., De Ridder et al. 2009; Hekker et al. 2009; Miglio et al. 2009; Carrier et al. 2010; Kallinger et al. 2010b; Miglio et al. 2010; Mosser et al. 2010; Hekker et al. 2010a) missions. Global oscillation parameters, such as $\nu_{\rm max}$ (the frequency of maximum oscillation power) and $\langle\Delta\nu\rangle$ (the average frequency separation between consecutive overtones of oscillation modes) together with the stellar effective temperature provide valuable information about the stars such as the mass and the radius. These parameters together with other stellar parameters available in the *Kepler* Input Catalogue (KIC, Batalha et al. 2010) give a more complete characterisation of the sample of stars at hand.

2 TARGET SELECTION

The Q0 timeseries alone are considered to be too short to determine global oscillation parameters, and only those stars for which Q1 timeseries are available have been analysed. This comprised a sample of 150 597 stars in total. From this sample of stars a subset of 16 511 red-giant stars have been selected using the definition of red giants provided by Ciardi et al. (2010):

$$\log g \leqslant 5.2 - 2.8 \cdot 10^{-4} T_{\rm eff}/{\rm K}, \quad (1)$$

⋆ E-mail: saskia@bison.ph.bham.ac.uk; A table with results is available upon request from the first author.

[1] http://archive.stsci.edu/pub/kepler/lightcurves/tarfiles/

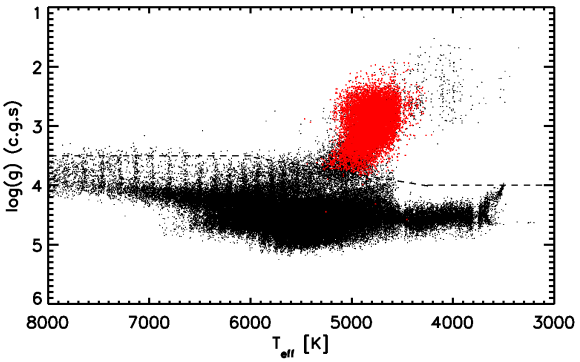

Figure 1. $\log g$ versus $T_{\rm eff}$ of all ~150 000 stars for which Q1 public data are available (black) and red giants in which oscillations have been detected (red). The dashed line indicates the division between red giants (low $\log g$) and other stars (high $\log g$) as described by Eq. 1.

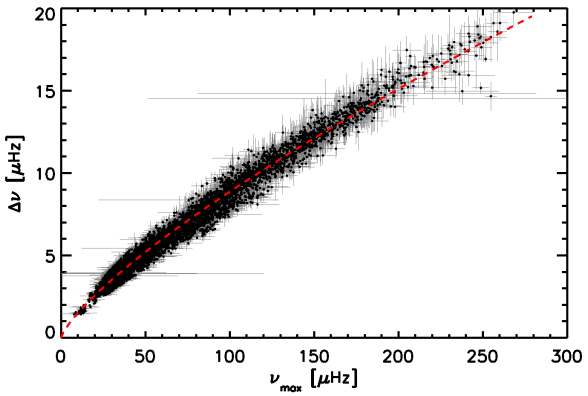

Figure 2. $\langle\Delta\nu\rangle$ versus $\nu_{\rm max}$ for the oscillating red giants. The red dashed line indicates the power-law fit through the results (see text).

for the range 4250 K $< T_{\rm eff} <$ 6000 K, and $\log g \leqslant 4$ for stars with $T_{\rm eff} <$ 4250 K (see Fig. 1).

The sample of stars investigated here is distinct from the set of oscillating red giants in *Kepler* data discussed in the several papers mentioned in the introduction. For the earlier papers, analyses used targets selected either as astrometric, red-giant control stars (about 1 000 uniformly distributed over the field of view with an apparent magnitude in the *Kepler* bandpass (Kp) ranging from 11.3 to 12.1), or a comparably large number of generally brighter giants that had been selected for observation by the Kepler Asteroseismic Science Consortium (KASC). In both cases these time series for Q1 were not included in the public data set analysed in this paper. These public data come from the *Kepler* science team targets selected on the basis of allowing planets to be detected if transiting these stars (Batalha et al. 2010).

3 RESULTS

Power spectra of the red-giant sample have been analysed using the analysis methods described by Hekker et al. (2010c). We already had at our disposal datasets on red-giant KASC targets that are of the same length as the public datasets. These KASC datasets have been analysed by several independent teams (Hekker et al. 2011, and references therein), from which, in general, consistent results were obtained. We can therefore have confidence that the results presented here, from one method, should be robust.

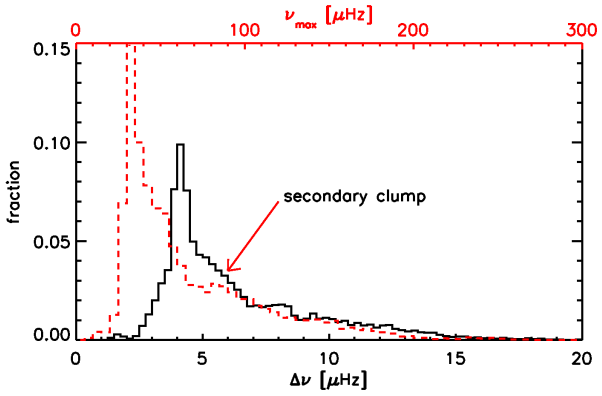

Figure 3. Distribution of $\nu_{\rm max}$ (red dashed line and top-axis) and $\langle\Delta\nu\rangle$ (black solid line and bottom axis).

3.1 Oscillation parameters

We expect a correlation between $\langle\Delta\nu\rangle$ and $\nu_{\rm max}$ (Hekker et al. 2009; Stello et al. 2009a; Mosser et al. 2010). This correlation is shown in Fig. 2 together with a polynomial fit of the form:

$$\langle\Delta\nu\rangle = a\nu_{\rm max}^{b}, \quad (2)$$

with $[a,b] = [0.257\pm0.002, 0.769\pm0.002]$ consistent with earlier results presented by Huber et al. (2010). The increased spread around the correlation at the high-end of the $\nu_{\rm max}$ relation is consistent with the expected spread due to stellar masses, which increases with $\nu_{\rm max}$ (see e.g. Hekker et al. 2010b; Huber et al. 2010; Stello et al. 2009a).

In Fig. 3, the fractional distributions of $\nu_{\rm max}$ and $\langle\Delta\nu\rangle$ values are shown. The large number of stars with 30 μHz $< \nu_{\rm max} <$ 50 μHz and $\langle\Delta\nu\rangle$ around 4 μHz are He-burning red-clump stars (Miglio et al. 2009). The additional smaller secondary hump at $\nu_{\rm max}$ between roughly 60 and 110 μHz, indicated with the red arrow, can be attributed to the secondary-clump (Miglio et al. 2009). The secondary-clump consists of He-burning stars with masses high enough to have ignited He in a non-degenerate core.

3.2 Stellar parameters

Following the approach by Kallinger et al. (2010b) we use the values of $\langle\Delta\nu\rangle$, $\nu_{\rm max}$ and the effective temperatures from the *Kepler* Input Catalog in combination with the scaling relations as described by Kjeldsen & Bedding (1995) to compute the masses and radii of the stars directly:

$$\nu_{\rm max} = 3120 \frac{M/M_{\odot}}{(R/R_{\odot})^2\sqrt{T_{\rm eff}/5777{\rm K}}}\mu{\rm Hz}, \quad (3)$$

$$\Delta\nu = 134.9\sqrt{\frac{M/M_{\odot}}{(R/R_{\odot})^3}}\mu{\rm Hz}, \quad (4)$$

using the solar values as determined by Kallinger et al. (2010a). From the radii and $T_{\rm eff}$ we computed the luminosity as $L \propto R^2T_{\rm eff}^4$. Using this luminosity, the apparent *Kepler* magnitude and the extinction coefficient (A_V, available in the KIC) we computed the dis-

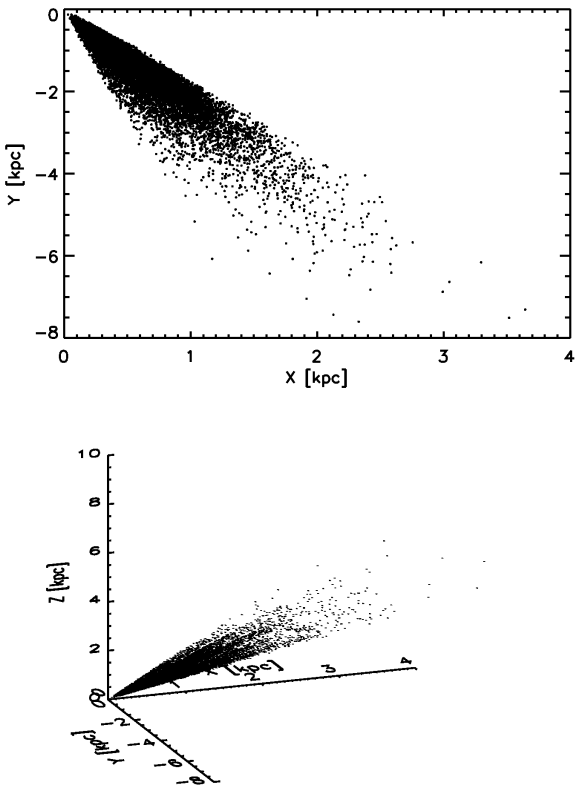

Figure 5. Positions of the public red-giant stars for which oscillations have been detected in the X-Y plane (top) and X-Y-Z space (bottom).

tances of the stars. Histograms of masses, radii, luminosities and distances are shown in Fig. 4.

The mass distribution has one clear peak between 1 and 2 $M_\odot$, while the distribution of the radii shows indications of a dominant peak located at ∼11 $R_\odot$. These peaks in the distributions are most likely due to stars in the red clump, i.e. He-burning stars (see Miglio et al. 2009, for a population study of red giants). The radius distribution shows an additional shoulder between roughly 5 and 8 $R_\odot$, which consists most likely of less evolved H-shell burning red giants ascending the giant branch.

The majority of the observed red giants have luminosities between 10 and 100 $L_\odot$ and reside at a distance between 1 and 5 kpc. The steep fall off for low luminosities / shorter distances and the gradual fall off in the number of stars at higher luminosities / larger distances are due to the magnitude range accessible with the *Kepler* satellite. The positions of the stars in the X-Y plane and X-Y-Z space, i.e., cartesian projections of the right ascension and declination, are shown in Fig. 5.

Note that the masses, radii, luminosities and distances computed from the direct method have relatively large uncertainties. These uncertainties are expected to broaden the distributions, but have minimal influence on the location of dominant peaks in the distributions (see Gai et al. (2010) for an in-depth investigation).

4 DISCUSSION

For 71% (11 805 out of 16 511) of the red giants, as defined by Ciardi et al. (2010), solar-like oscillations could be detected. Comparing this fraction with the performance of CoRoT, we see that Mosser et al. (2010) detect oscillations in 39% of the red-giant candidates. This shows the importance of the increased signal-to-noise ratio of *Kepler* observations, which include targets in the apparent magnitude range 8-14 mag, compared to CoRoT observations with targets with apparent magnitudes ranging between 11 and 16 mag.

What could be the reason that we do not detect oscillations in the other 29% of the stars? This could be either due to analysis or observation biases, or due to intrinsic effects in the stars. All stars have been analysed with an automated method (Hekker et al. 2010c) and checked by eye. This should make sure that the detection of solar-like oscillations is not significantly influenced by the automation. The observations are such that we are able to observe oscillations with $\nu_{\rm max}$ only in the range between roughly 10 and 250 μHz. The lower limit is due both to the frequency resolution and to the presence of low frequency signatures, among which granulation, present in the power spectra. The upper limit is set by the Nyquist frequency of ∼283 μHz. From the $\log g$ and effective temperature we computed a prediction for $\nu_{\rm max}$ for the stars for which no oscillations were detected. For ∼4200 stars the predicted $\nu_{\rm max}$ were indeed outside the frequency range for which the current data are sensitive. Furthermore, artefacts such as the signature of the cycling of the heater on one of the *Kepler* reaction wheels (as already reported by Hekker et al. 2011, and in the *Kepler* data release notes) might also hamper the detection of the oscillations. Contamination from other instrumental effects or photon-shot noise may also be relevant. Additionally, we found during the manual check that there are some binaries and classical oscillators present in the sample which features hamper the detection of solar-like oscillations. Note that for binaries the KIC estimate of $T_{\rm eff}$ and $\log g$ are rather doubtful. Prsa et al. (2010) give a conservative estimate of only 1.2% eclipsing binaries in the sample.

For longer timeseries the fraction of stars with detected oscillations will increase due to the increased sensitivity to longer oscillation periods and due to the reduction of the noise. Note also that the reaction wheel artefact is much less pronounced in data from runs obtained after Q1.

4.1 Populations

For a further investigation of the population of red giants for which oscillations have been detected we show $\nu_{\rm max}$ versus $\nu_{\rm max}/\langle\Delta\nu\rangle$ in Fig. 6, in the same way as Huber et al. (2010), but now with colour-coding for mass, radius, luminosity and effective temperature also included. The mass, radius and luminosity of the stars in this diagram show smooth transitions with the global oscillation parameters, as predicted from stellar models. However the trends in global oscillation parameters appear to be almost independent of effective temperature. In the same figure, we also show H-R diagrams colour-coded for radius and mass, and mass versus radius diagrams colour-coded for luminosity and effective temperature.

We note that the positions of the stars in the H-R diagram shown here are biased in effective temperature and luminosity compared to the CoRoT results (see Fig. 15 of Mosser et al. 2010). This could indicate either an overestimate of the red-giant effective temperatures in the *Kepler* input catalogue, or an underestimate of the effective temperatures of CoRoT. The results shown in Fig. 6 are in agreement with the population study by Miglio et al. (2009).

We can identify some specific stages of stellar evolution in these diagrams:

- The majority of stars with 25 μHz < $\nu_{\rm max}$ < 45 μHz with

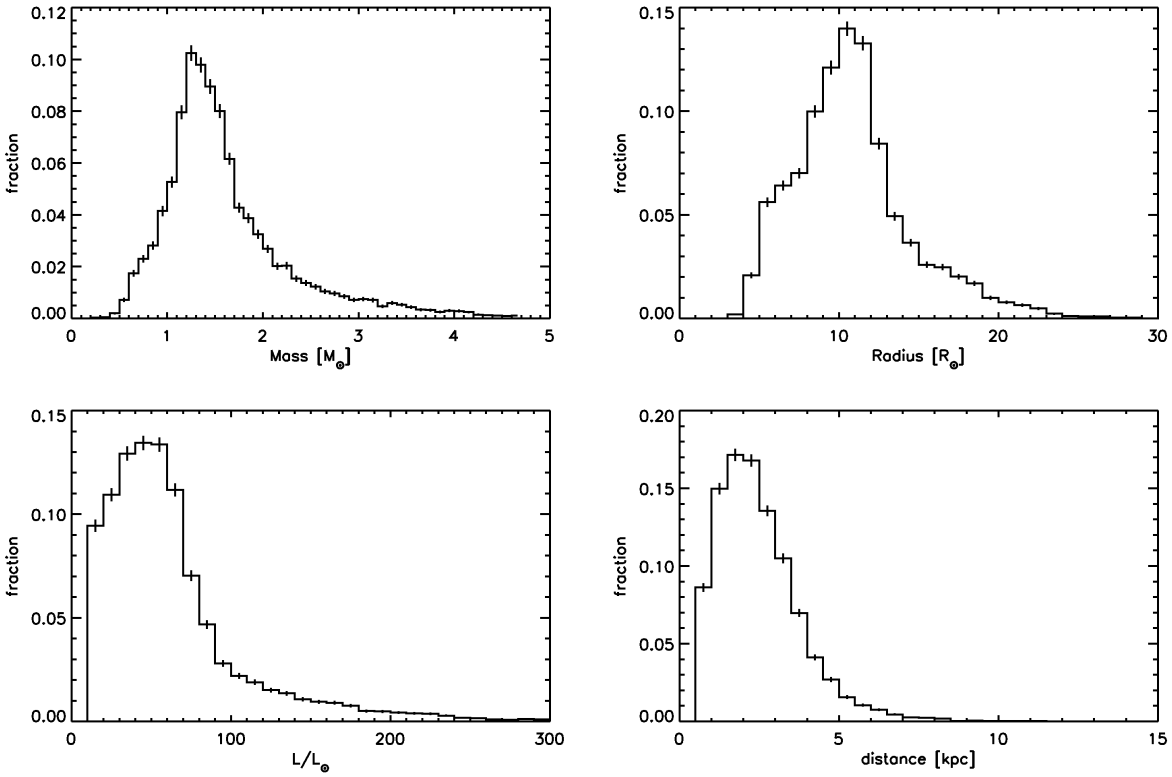

Figure 4. Fractional distributions of asteroseismic masses (left top), radii (right top), luminosities (left bottom) and distances (right bottom) of the red giants with detected solar-like oscillations in the public data. Uncertainties computed assuming Poisson statistics are indicated.

masses roughly below 2 $M_\odot$ are known to be He-core burning stars that have gone through the Helium flash. These stars have radii of ~10 $R_\odot$ and $\log L/L_\odot$ of ~2 and are the so-called *red-clump stars* (see e.g., Miglio et al. 2009; Huber et al. 2010; Kallinger et al. 2010a; **?**, for previous detections of the red clump).

- The stars in the lower radius shoulder in the radius distribution (Fig. 4) all have low luminosities and lay in the H-R diagram (panel G in Fig. 6) below the black dashed line indicating stars with radii of 7.5 $R_\odot$. We identify this population as *low-luminosity red-giant branch stars*.
- At $\nu_{\rm max} < 25$ μHz a group of stars with low effective temperatures is present (see panel B in Fig. 6). These stars also have relatively high luminosities (see panel D) and large radii (see panel C), and low to intermediate masses (see panel A). We identify these stars as *high-luminosity red-giant branch stars* or *asymptotic giant branch stars*.
- There is some evidence for the secondary clump. Stars with masses roughly between 2 and 3 $M_\odot$ and radii between 7.5 and 10 $R_\odot$ seem to form a separate branch in the mass versus radius diagram with slightly increased temperatures (panel F in Fig. 6). These stars are also visible in the $\nu_{\rm max}$ versus $\nu_{\rm max}/\langle\Delta\nu\rangle$ diagram and in the $\nu_{\rm max}$ histogram (Fig. 3) at the expected location of the secondary clump (Girardi 1999; Huber et al. 2010; Kallinger et al. 2010a). These are stars in their He-burning phase, which are massive enough to have ignited He-burning in a non-degenerate core. We therefore identify these stars as *secondary-clump stars*.
- The high-mass stars (> 3.75 $M_\odot$) form a distinct group of stars at high $\nu_{\rm max}/\langle\Delta\nu\rangle$ and $\nu_{\rm max}$ values similar to the red-clump stars (see panel A of Fig. 6). These stars also have large radii, high luminosities.

Additionally, there seems to be a rather steep fall-off for stars with masses greater than roughly 2 $M_\odot$ at $\nu_{\rm max} \sim 110$ μHz (panel A of Fig. 6). This indicates the maximum $\nu_{\rm max}$ of He-burning stars and the region with larger $\nu_{\rm max}$ is populated exclusively with H-shell burning red giant branch stars (Miglio et al. 2009). The lack of high-mass stars in the red-giant branch is consistent with high-mass stars evolving much faster than their low-mass counter parts during the H-shell burning phase.

The different populations identified above are indicated in the H-R diagram, mass versus radius diagram and $\nu_{\rm max}$ versus $\nu_{\rm max}/\langle\Delta\nu\rangle$ diagram in the left column of Fig. 7. Two distinct unidentified regions are still apparent in the H-R diagram, i.e. the black dots above and below the red clump. The more luminous stars have masses between 2 and 3.75 $M_\odot$ and $\nu_{\rm max}$ between 25 and 80 μHz, which could be either in the H-shell or He-core/H-shell burning stars. The stars below the the red clump are stars with $M < 2$ $M_\odot$, $R > 7.5$ $R_\odot$ and $\nu_{\rm max} > 45$ μHz. These are most likely stars in the H-shell burning phase ascending the red-giant branch.

For the analysis described above we used the KIC effective temperatures and derived masses and radii directly from the scaling relations (Eq. 3 and 4). We now compare these results with results from a grid-based approach using information from a grid of models to compute the seismic effective temperatures, masses, radii and luminosities of the stars (Kallinger et al. 2010a). In the grid-based approach stellar evolution is taken into account, while the scaling relations assume that all values of $T_{\rm eff}$ are possible for a star of a given mass and radius. Using the grid-based approach should therefore reduce the uncertainties of the determined parameters (see also Gai et al. 2010). The results from the grid-based approach are shown in the right column of Fig. 7. The grid-based

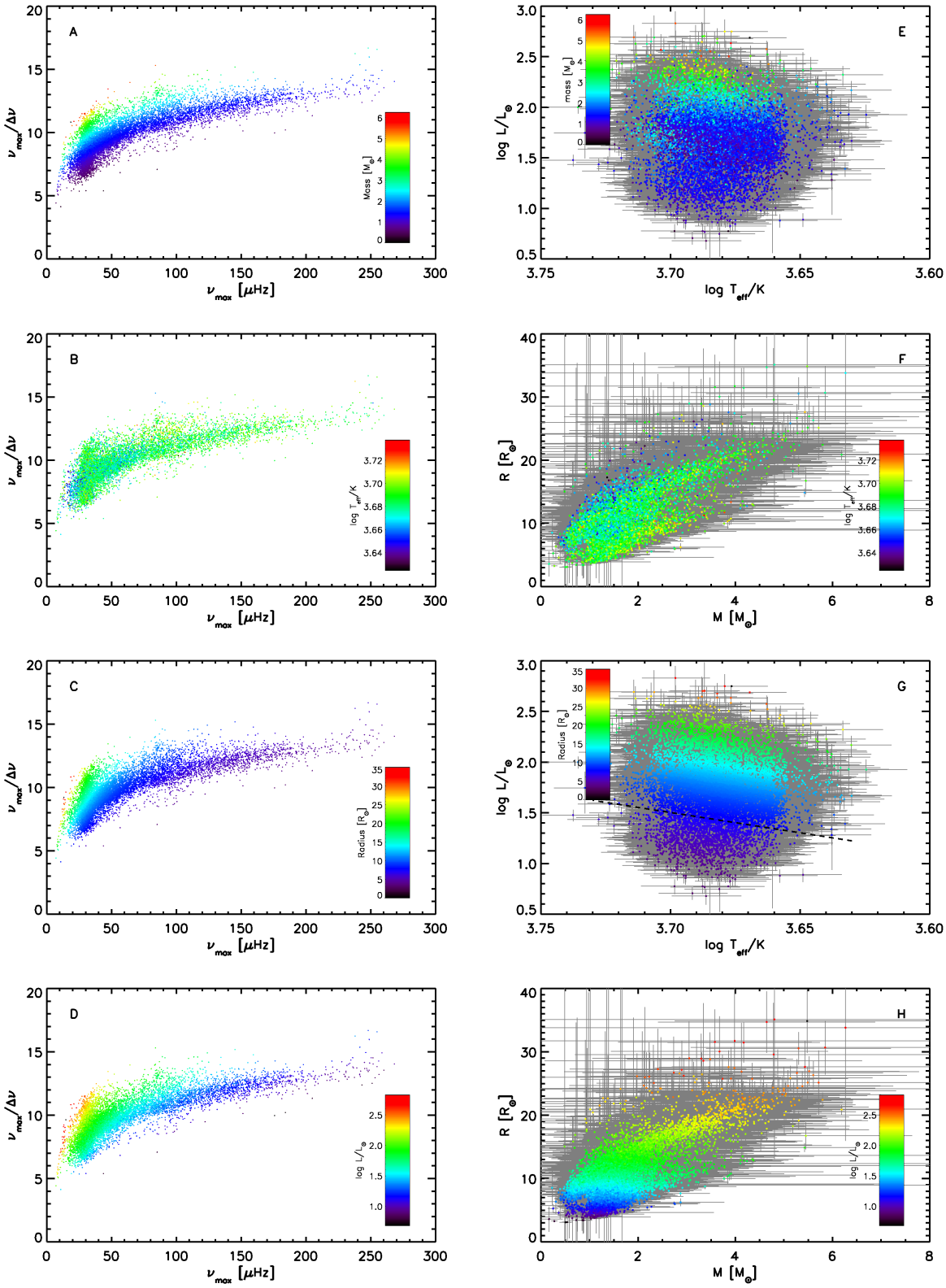

Figure 6. $\nu_{\rm max}$ versus $\nu_{\rm max}/\langle\Delta\nu\rangle$ diagrams (left) and H-R diagrams and mass versus radius diagrams (right) of the public red giants with detected oscillations. The colour-coding indicates from top to bottom mass, effective temperature, radius and luminosity. Error bars are indicated in gray in the H-R diagrams and mass versus radius diagrams and omitted in the $\nu_{\rm max}$ versus $\nu_{\rm max}/\langle\Delta\nu\rangle$ diagrams for visual purposes.

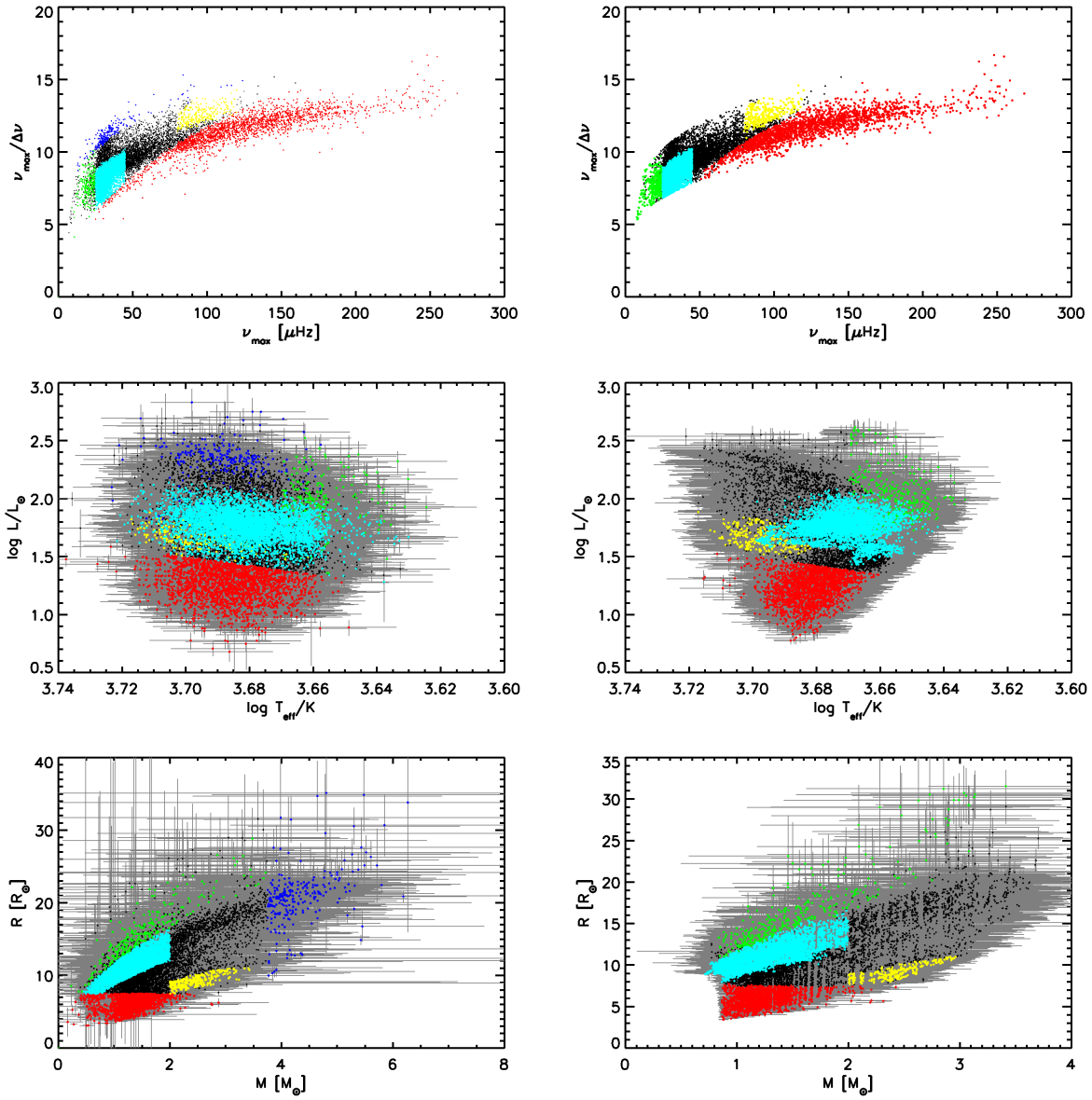

Figure 7. $\nu_{\rm max}$ versus $\nu_{\rm max}/\langle\Delta\nu\rangle$ diagrams (top), H-R diagrams (centre) and mass versus radius diagrams (bottom) of the public red giants with detected oscillations analysed using the direct method (left) and grid-based approach (right). The different identified populations are indicated with different colours: *low-luminosity red-giant branch stars* in red, *red-clump stars* in cyan, *secondary-clump stars* in yellow, *high-luminosity red-giant branch stars / asymptotic giant branch stars* in green and high-mass stars in dark blue. Stars which could not be assigned to a certain population are indicated with black dots. Error bars are indicated in gray in the H-R diagrams and mass versus radius diagrams and omitted in the $\nu_{\rm max}$ versus $\nu_{\rm max}/\langle\Delta\nu\rangle$ diagrams for visual purposes.

approach indeed improves the structure in the H-R diagram, mass versus radius diagram and $\nu_{\rm max}$ versus $\nu_{\rm max}/\langle\Delta\nu\rangle$ diagram, but does not alter the identification of the different populations, except for the high-mass population. The stars with masses between 4 and 6 M$_\odot$ as computed from the direct method have all been corrected to have masses with $M < 4$ M$_\odot$ and are no longer a distinct population. These corrections indicate that for the stars with highest masses the uncertainties in the KIC and the direct method overestimate the stellar masses.

4.2 Effectiveness of oscillation detection

The fraction of red giants for which oscillations have been detected has its maximum at roughly $\log g = 2.7$ and $T_{\rm eff} = 4800$ K and decreases for higher and lower values of $\log g$ and $T_{\rm eff}$ (see Fig. 8). There is a notable absence of stars with detected oscillations in the region with $T_{\rm eff} < 4200$ K (right top corner in Fig. 8). These are the coolest stars with lowest $\log g$. These stars have very large radii and are expected to have long oscillation periods, for which (as stated above) the timespan of the Q1 data are not sufficient. It is also clear that for hotter stars ($T_{\rm eff} > 5200$ K) with higher gravity ($\log g > 3$) less oscillating stars have been detected. These stars are in a less evolved state, in which possible solar-like oscillations occur at frequencies higher than the Nyquist frequency (283 μHz)

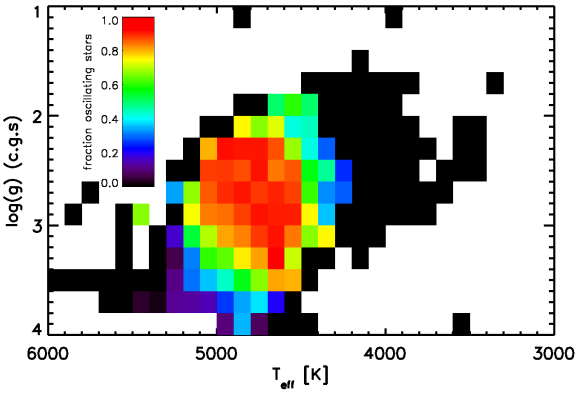

Figure 8. Zoom of Fig. 1 into the red-giant range showing the fraction of red giants with detected solar-like oscillations in $\log g$ versus $T_{\rm eff}$. Each square represents an interval of 0.2 dex in $\log g$ and 100 K in $T_{\rm eff}$.

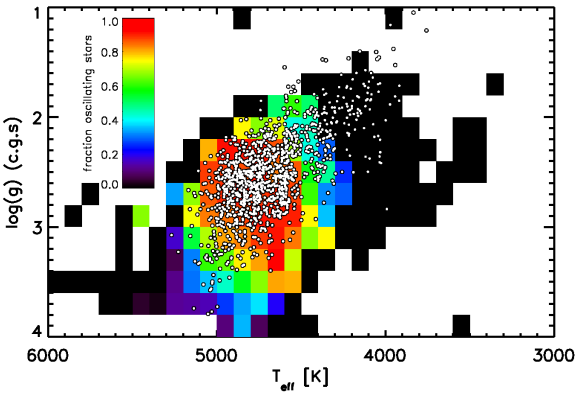

Figure 9. Same as Fig. 8 with the location of the red-giant stars analysed within the Kepler Asteroseismic Science Consortium (see text) shown (white dots).

of the long cadence *Kepler* data, investigated here. We also checked the fraction of detections as a function of magnitude, and this shows no clear trend. The ratios of stars in each magnitude interval with detected oscillations to stars without detections are very similar. This shows that the detection of solar-like oscillations in red-giant stars does not depend (strongly) on the apparent magnitude. Note that there are only a few red giants brighter than 8$^{\rm th}$ magnitude and no red-giant stars fainter than 14$^{\rm th}$ magnitude present among the public data.

We have compared the population of red giants in the public data described here with the red giants analysed within the Kepler Asteroseismic Science Consortium (KASC) (Bedding et al. 2010; Hekker et al. 2011; Huber et al. 2010; Kallinger et al. 2010a). The KASC stars are shown with white dots in Fig. 9. It is clear that a large fraction of these stars are located in the same $T_{\rm eff}$ - $\log g$ range as the public data on stars showing oscillations, although the lower right corner of the red/orange region indicating a high fraction (>80%) of detected oscillators in the public data is not well populated with KASC stars. There are also many fewer oscillating KASC red giants with $\log g > 3.5$. The lack of KASC stars in both regions could possibly be caused by selection effects, and low number statistics due to the fact that in these regions in the H-R diagram stars evolve relatively rapidly and thus that the chance of observing a star in this region is lower. Indeed the astrometric control set, the largest component of KASC analysed red giants, was selected to have large distances, hence small $\log g$. Finally, in the low $\log g$ - low $T_{\rm eff}$ range where hardly any oscillations have been detected in the public data, we see a non-negligible number of oscillating KASC stars. This is most likely due to the fact that the KASC timeseries analysed are three months longer than the public data analysed here.

4.3 Variability

We checked for possible correlations between the stellar variability and the detection of solar-like oscillations in red-giant stars. To investigate the possible influence of intrinsic stellar effects, like for instance the presence of a magnetic field or 'solar cycle' as expected for main-sequence stars (Chaplin et al. 2010), on the detectability of oscillations, we computed the standard deviation of each smoothed lightcurve. We applied a triangular-shaped filter with a FWHM of five days. The results are shown for all red giants in Fig. 10. In Fig. 10 we also show the 'minimal noise' level for *Kepler* as defined by Jenkins et al. (2010b):

$$\sigma = \sqrt{c + 7 \times 10^6 \max(1, Kp/14)^4}/c, \qquad (5)$$

with Kp the *Kepler* magnitude and $c = 3.46 \times 10^{0.4(12-Kp)+8}$. Gilliland (2008) using HST observations of the galactic bulge found a similar degree of excess variability in giants (based on position in CMD) relative to dwarfs.

From Fig. 10 it becomes clear that the stars with detected oscillations and without detected oscillations cover a very similar range of long-term variability. From this we conclude that there is no correlation between stellar variability with time scales longer than 5 days and the detection of solar-like oscillations in red-giant stars.

4.4 Surface gravity

For the analyses carried out in this work, $\log g$ values from the *Kepler* Input Catalogue have been used, because those values are available for stars with and without detected oscillations. It is however interesting to compare the KIC $\log g$ with $\log g$ computed from asteroseismology. Figure 11 shows the KIC $\log g$ as a function of $\log g_{\rm seismic}$ with $g_{\rm seismic} \propto T_{\rm eff}^{0.5} \nu_{\rm max}$, in which $T_{\rm eff}$ values from the KIC have been used. This Figure shows that the values in the KIC are in general consistent or higher than the values obtained using asteroseismology. The spread in $\log g_{\rm seismic}$ is notably smaller than in the KIC values with the majority of the stars having $\log g_{\rm seismic}$ roughly between 2.3 and 2.7. This concentration indicates the red clump with He-core burning stars, while the stars with higher $\log g_{\rm seismic}$, i.e., > 2.7 are the *low-luminosity red-giant branch stars* and the stars with lower $\log g_{\rm seismic}$, i.e., < 2.2, the *high-luminosity red-giant branch stars* or *asymptotic giant branch stars*.

Note that the uncertainties in the results for $\log g_{\rm seismic}$ are considerably smaller than the uncertainties in the KIC $\log g$ values. This has been predicted by Gai et al. (2010). They show that $\log g_{\rm seismic}$ is a very robust parameter with uncertainties of only a few percent.

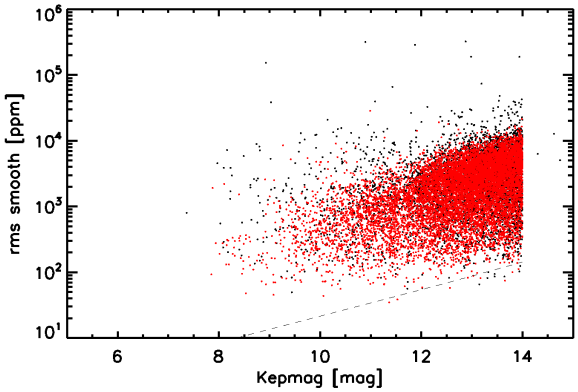

Figure 10. The standard deviation of the smoothed light curves for red giants with detected oscillations (red) and red giants without detected oscillations (black). The gray dashed line indicates the 'minimal noise' level (see text).

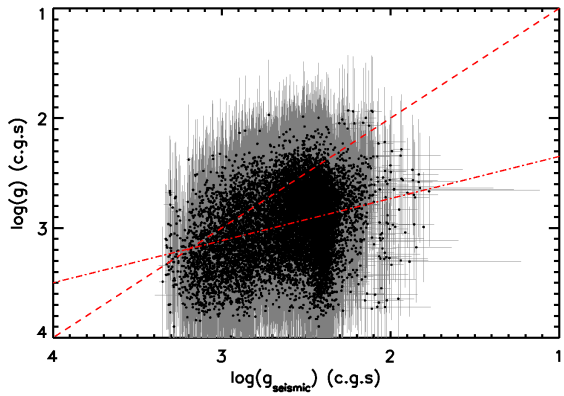

Figure 11. log g of the *Kepler* Input Catalogue as a function of log $g_{\rm seismic}$ determined from asteroseismic parameters. Uncertainties are indicated in gray. The red dashed line shows the one-to-one relation and the red dashed-dotted line a linear fit through the data.

5 SUMMARY

The 33 days of public *Kepler* data observed in Q1 have been investigated for solar-like oscillations in red-giant stars. For 71% of the red giants, oscillations could be detected and for these stars asteroseismic masses, radii, luminosities and distances have been derived. These are computed directly from scaling relations (Eqs. 3 and 4) and in a second analysis using a grid-based approach (Stello et al. 2009b; Kallinger et al. 2010a; Gai et al. 2010; Basu et al. 2010).

The stellar parameters determined with the direct method from the relatively short timeseries are accurate enough to distinguish between different populations of stars, i.e., *low-luminosity red-giant branch stars* and *high-luminosity red-giant branch stars* in the H-shell burning phase or *asymptotic giant branch stars*, He-core burning *clump* and *secondary-clump* stars. Furthermore, the lack of high-mass stars with high $\nu_{\rm max}$ (> 110 μHz) confirms observationally the theoretically known difference in evolutionary timescales between stars of different masses.

The fact that we did not detect oscillations for 29% of the red giants in the sample can be explained by observational influences, such as the limited timespan of the data and instrumental artefacts. No correlation with detectability could be determined with the apparent magnitude of the stars. Over the next few years when more data will become available and minor problems with instrumental artefacts overcome, we expect to observe solar-like oscillations in a larger fraction of the giants. CoRoT observations spanning about 150 days have shown that more than 75% of the red-giant candidates with apparent magnitude brighter than 13$^{\rm th}$ magnitude show oscillations (**?**).

Finally, we investigated the correlation between long-term variability of the red giants with and without oscillations. No clear correlation could be detected, which indicates that the detection of solar-like oscillations in red giants does not depend on the long-term variability of the star caused e.g. by stellar activity.

ACKNOWLEDGEMENTS

The authors gratefully acknowledge the *Kepler* Science Team and all those who have contributed to making the *Kepler* mission possible. Funding for this Discovery mission is provided by NASA's Science Mission Directorate. SH, YE and WJC acknowledges financial support from the UK Science and Technology Facilities Council (STFC).

REFERENCES

Basu S., Grundahl F., Stello D., Kallinger T., Hekker S., Mosser B., 2010, submitted to ApJ
Batalha N. M., Borucki W. J., Koch D. G., Bryson S. T., Haas M. R., Brown T. M., Caldwell D. A., Hall J. R., Gilliland R. L., Latham D. W., Meibom S., Monet D. G., 2010, ApJ, 713, L109
Bedding T. R., Huber D., Stello D., Elsworth Y. P., Hekker S., Kallinger T., Mathur S., Mosser B., Preston H. L., Ballot J., Barban C., Broomhall A. M., et al. 2010, ApJ, 713, L176
Borucki W., Koch D., Batalha N., Caldwell D., Christensen-Dalsgaard J., Cochran W. D., Dunham E., Gautier T. N., Geary J., Gilliland R., Jenkins J., Kjeldsen H., Lissauer J. J., Rowe J., 2009, in IAU Symposium Vol. 253 of IAU Symposium, KEPLER: Search for Earth-Size Planets in the Habitable Zone. pp 289–299
Carrier F., De Ridder J., Baudin F., Barban C., Hatzes A. P., Hekker S., Kallinger T., Miglio A., Montalbán J., Morel T., Weiss W. W., Auvergne M., Baglin A., Catala C., Michel E., Samadi R., 2010, A&A, 509, A73
Chaplin W., Bedding T., Bonanno A., Broomhall A.-M., García R., Hekker S., Huber D., 2010, submitted to ApJ
Ciardi D. R., von Braun K., Bryden G., van Eyken J., Howell S. B., Kane S. R., Plavchan P., Stauffer J. R., 2010, ArXiv e-prints: 1009.1840, submitted to AJ
De Ridder J., Barban C., Baudin F., Carrier F., Hatzes A. P., Hekker S., Kallinger T., Weiss W. W., Baglin A., Auvergne M., Samadi R., Barge P., Deleuil M., 2009, Nature, 459, 398
Gai N., Basu S., Chaplin W. J., Elsworth Y., 2010, ArXiv e-prints:1009.3018, submitted to ApJ
Gilliland R. L., 2008, AJ, 136, 566
Girardi L., 1999, MNRAS, 308, 818
Hekker S., 2010, ArXiv e-prints:1006.4390, AN in press
Hekker S., Barban C., Baudin F., De Ridder J., Kallinger T., Morel T., Chaplin W. J., Elsworth Y., 2010a, A&A, 520, A60
Hekker S., Basu S., Stello D., Kallinger T., Grundahl F., 2010b, submitted to A&A

Hekker S., Broomhall A., Chaplin W. J., Elsworth Y. P., Fletcher S. T., New R., Arentoft T., Quirion P., Kjeldsen H., 2010c, MNRAS, 402, 2049

Hekker S., Debosscher J., Huber D., Hidas M. G., De Ridder J., Aerts C., Stello D., Bedding T. R., Gilliland R. L., Christensen-Dalsgaard J., Brown T. M., Kjeldsen H., Borucki W. J., Koch D., Jenkins J. M., 2010d, ApJ, 713, L187

Hekker S., Elsworth Y., De Ridder J., Mosser B., Garcia R. A., Kallinger T., Mathur S., Huber D., Buzasi D. L., Preston H. L., Hale S. J., Ballot J., Chaplin W. J., Regulo C., Bedding T. R., Stello D., et al. 2011, A&A, 525, A131

Hekker S., Kallinger T., Baudin F., De Ridder J., Barban C., Carrier F., Hatzes A. P., Weiss W. W., Baglin A., 2009, A&A, 506, 465

Huber D., Bedding T. R., Stello D., Mosser B., Mathur S., Kallinger T., Hekker S., Elsworth Y. P., Buzasi D. L., De Ridder J., Gilliland R. L., et al. 2010, ApJ, 723, 1607

Jenkins J. M., Caldwell D. A., Chandrasekaran H., Twicken J. D., Bryson S. T., Quintana E. V., Clarke B. D., Li J., Allen C., Tenenbaum P., Wu H., Klaus T. C., Middour C. K., et al. 2010a, ApJ, 713, L87

Jenkins J. M., Caldwell D. A., Chandrasekaran H., Twicken J. D., Bryson S. T., Quintana E. V., Clarke B. D., Li J., Allen C., Tenenbaum P., Wu H., Klaus T. C., Van Cleve J., Dotson J. A., Haas M. R., Gilliland R. L., Koch D. G., Borucki W. J., 2010b, ApJ, 713, L120

Kallinger T., Mosser B., Hekker S., Huber D., Stello D., Mathur S., Basu S., Bedding T. R., Chaplin W. J., De Ridder J., Elsworth Y. P., et al. 2010a, A&A, 522, A1

Kallinger T., Weiss W. W., Barban C., Baudin F., Cameron C., Carrier F., De Ridder J., Goupil M., Gruberbauer M., Hatzes A., Hekker S., Samadi R., Deleuil M., 2010b, A&A, 509, A77

Kjeldsen H., Bedding T. R., 1995, A&A, 293, 87

Miglio A., Montalbán J., Baudin F., Eggenberger P., Noels A., Hekker S., De Ridder J., Weiss W., Baglin A., 2009, A&A, 503, L21

Miglio A., Montalbán J., Carrier F., De Ridder J., Mosser B., Eggenberger P., Scuflaire R., Ventura P., D'Antona F., Noels A., Baglin A., 2010, A&A, 520, L6

Mosser B., Belkacem K., Goupil M., Michel E., Elsworth Y., Barban C., Kallinger T., Hekker S., De Ridder J., Samadi R., Baudin F., Pinheiro, F.J.G., Auvergne M., Baglin A. & Catala C., 2011, A&A, 525, L9

Mosser B., Belkacem K., Goupil M., Miglio A., Morel T., Barban C., Baudin F., Hekker S., Samadi R., De Ridder J., Weiss W., Auvergne M., Baglin A., 2010, A&A, 517, A22

Prsa A., Batalha N. M., Slawson R. W., Doyle L. R., Welsh W. F., Orosz J. A., Seager S., Rucker M., Mjaseth K., Engle S. G., Conroy K., Jenkins J. M., Caldwell D. A., Koch D. G., Borucki W. J., 2010, ArXiv e-prints

Samadi R., Georgobiani D., Trampedach R., Goupil M. J., Stein R. F., Nordlund Å., 2007, A&A, 463, 297

Stello D., Chaplin W. J., Basu S., Elsworth Y., Bedding T. R., 2009a, MNRAS, 400, L80

Stello D., Chaplin W. J., Bruntt H., Creevey O. L., García-Hernández A., Monteiro M. J. P. F. G., Moya A., Quirion P., Sousa S. G., Suárez J., et al. 2009b, ApJ, 700, 1589